Mechanistic insights on novel small molecule allosteric activators of cGMP-dependent protein kinase PKG1α

Paul Tawa[1], Lei Zhang[2], Essam Metwally[3], Yan Hou[1], Mark A. McCoy[1], W. Michael Seganish[4], Rumin Zhang[1], Emily Frank[5], Payal Sheth[1], Jennifer Hanisak[6], Christopher Sondey[7], David Bauman[8], and Aileen Soriano[1],*

From the [1]Mass Spectrometry & Biophysics, Computational & Structural Chemistry, and [2]Biologics AR&D Immunoassay Group, Merck & Co, Inc, Kenilworth, New Jersey, USA; [3]Computational & Structural Chemistry, and [4]Discovery Chemistry, Merck & Co, Inc, South San Francisco, California, USA; [5]Quantitative Biosciences, and [6]Discovery Chemistry, Merck & Co, Inc, Kenilworth, New Jersey, USA; [7]Quantitative Biosciences, Merck & Co, Inc, Boston, Massachusetts, USA; [8]Discovery Biology, Merck & Co, Inc, Kenilworth, New Jersey, USA

Edited by Henrik Dohlman

cGMP-dependent protein kinase (PKG) represents a compelling drug target for treatment of cardiovascular diseases. PKG1 is the major effector of beneficial cGMP signaling which is involved in smooth muscle relaxation and vascular tone, inhibition of platelet aggregation and signaling that leads to cardioprotection. In this study, a novel piperidine series of activators previously identified from an ultrahigh-throughput screen were validated to directly bind partially activated PKG1α and subsequently enhance its kinase activity in a concentration-dependent manner. Compounds from initial optimization efforts showed an ability to activate PKG1α independent of the endogenous activator, cGMP. We demonstrate these small molecule activators mimic the effect of cGMP on the kinetic parameters of PKG1α by positively modulating the K_M of the peptide substrate and negatively modulating the apparent K_M for ATP with increase in catalytic efficiency, k_{cat}. In addition, these compounds also allosterically modulate the binding affinity of cGMP for PKG1α by increasing the affinity of cGMP for the high-affinity binding site (CNB-A) and decreasing the affinity of cGMP for the low-affinity binding site (CNB-B). We show the mode of action of these activators involves binding to an allosteric site within the regulatory domain, near the CNB-B binding site. To the best of our knowledge, these are the first reported non-cGMP mimetic small molecules shown to directly activate PKG1α. Insights into the mechanism of action of these compounds will enable future development of cardioprotective compounds that function through novel modes of action for the treatment of cardiovascular diseases.

The cGMP signaling pathway is impaired in cardiovascular diseases (1–4). Targeting this pathway with the aim of restoring the beneficial effects of the signaling cascade represents an important and clinically validated therapeutic strategy. Modulation of the cGMP pathway has been successfully translated in the clinic by use of cGMP-elevating agents that work by enhancing the activity of cGMP-generating enzymes (soluble and particulate guanylate cyclases, nitric oxide enhancers) or by blocking cGMP degradation through inhibition of phosphodiesterase activity (5–7). Riociguat (soluble guanylate cyclase stimulator) and sildenafil (phosphodiesterase 5 inhibitor), for example, were both approved for the treatment of pulmonary arterial hypertension while Vericiguat (soluble guanylate cyclase stimulator) was recently approved for chronic heart failure.

cGMP-dependent protein kinase (PKG) is the major effector of cGMP signaling in the cardiovascular system (1–4). PKG is involved in regulating physiological processes that includes smooth muscle relaxation and vascular tone (8), inhibition of platelet aggregation (9), and signaling that lead to cardioprotection (1–4). PKG therefore represents a compelling drug target for treatment of cardiovascular diseases. Direct pharmacological activation of PKG, independent of cGMP, may capture the beneficial effects of cGMP-PKG signaling while bypassing the multiple downstream signaling pathways mediated by other cGMP effectors (10).

PKG1 is a soluble homodimer and is the main PKG isoform in the cardiovascular system (11). It exists as two splice variants, PKG1α and PKG1β, that differ in the first 100 amino acids of their sequence, which imparts differential affinity for cGMP as well as protein substrate specificity (11, 12). The PKG1 polypeptide is divided into two major domains: a regulatory domain and a catalytic domain (Fig. 1). The regulatory domain is comprised of functional subdomains (13–17). At the N terminus is a coiled coil leucine zipper responsible for homodimerization and subcellular localization of the protein. Following the leucine zipper is an autoinhibitory (AI) subdomain that contains an inhibitory motif called the "pseudosubstrate" motif (14, 15). The AI subdomain, in the absence of cGMP, interacts with the catalytic domain blocking substrate access and thus locking PKG in the basal, inactive state. Next to the AI subdomain are two tandemly arranged high and low
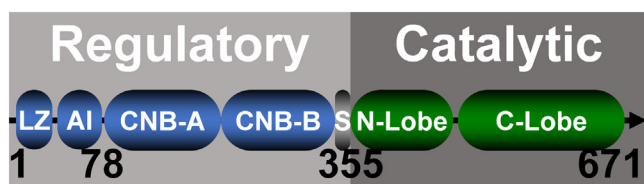
Figure 1. PKG1α domain organization. PKG1α is divided into regulatory (*blue*) and catalytic (*green*) regions. The regulatory region is comprised of a leucine zipper (LZ) domain, autoinhibitory domain (AI), cGMP high affinity binding domain (CNB-A), cGMP low affinity binding domain (CNB-B), and the switch helix (S). The catalytic region is subdivided into two domains: the Mg^{2+}/ATP-binding domain (N-lobe) and the protein substrate binding domain (C-lobe). CNB, cyclic nucleotide binding domain; PKG, cGMP-dependent protein kinase.

affinity cyclic nucleotide binding domain (CNB) sites (CNB-A and CNB-B, respectively) capable of binding cGMP and cAMP. In PKG1α, the high-affinity CNB-A lies closer to the N terminus (16). Following the CNB sites is a helical subdomain (switch helix, S) proposed to be involved in the regulation of kinase activity (17, 18). The C-terminal tail of the switch helix ('knob' site) interacts with the hydrophobic ('nest') site adjacent to the cGMP-binding site in CNB-B (17). Elements of this 'knob/nest' interaction are conserved in PKG1 (18). Site-directed mutagenesis of key residues in the 'knob' site in full-length PKG1α increased the basal activity of the kinase, decreased the activation constant for cGMP, and abolished cGMP-induced enzyme activation cooperativity. All of these suggest the involvement of the switch helix interactions in regulating enzyme activity (17).

The C-terminal catalytic region of PKG1 is comprised of two lobes: the N-terminal (N-) lobe, which contains the Mg^{2+}/ATP-binding site, and the C-terminal (C-) lobe, which contains the protein substrate-binding site (19). Activation of PKG1 requires binding of cGMP to the CNB sites triggering a significant conformational change that results in switching from a compact ball-like folded form in the basal (cGMP-free) inactive state to an extended and functionally active conformation that releases the catalytic domain from autoinhibition to allow phosphorylation of downstream protein substrates (16, 20).

To date, efforts to develop small molecule activators of PKG1 were focused on analogs of cGMP that are susceptible to off-target activity with limited pharmaceutical developability (21). Peptide-based activators of PKG1α were recently reported and were shown to inhibit myogenic constriction in smooth muscle cells in isolated, endothelium-denuded cerebral arteries (22). These peptides were derived from the sequence of the switch helix (S) bridging CNB-B and the catalytic domain and were proposed to activate PKG1α by disrupting the switch helix interactions involved in regulating kinase activity (22). Here, we describe the characterization of small molecule activators of PKG1α initially identified from an ultrahigh-throughput screening (uHTS) campaign (23). Early optimization efforts showed emerging potency to directly activate PKG1α from the basal state. By evaluating the modulation of cGMP binding to the high affinity (CNB-A) and low affinity (CNB-B) sites, we show that these compounds activate PKG1α by binding to a unique site allosteric to the two CNB sites within the regulatory domain of PKG1α.

Results

Enhancement of PKG1α kinase activity by small molecule activators

To search for direct activators of PKG1α, we implemented a uHTS screen that resulted in the discovery of small molecule activators **1** and **2** (Fig. 2). Early optimization efforts led to the synthesis of **21** and **23** (Fig. 2) (23). All four compounds could increase the enzymatic activity of the partially activated, full-length, recombinant PKG1α ($PKG1α_{2-671}$) in a concentration-dependent manner (Fig. 3A) with EC_{50} values between 5 μM and 47 μM (Table 1). These activation potencies were benchmarked against maximal PKG1α activity in the presence of cGMP that has an $EC_{50} \sim 0.03$ μM (Fig. 3A). The screen hits (**1** and **2**) did not show significant activation of the basal state of PKG1α within the concentration range tested (Fig. 3B), which was limited by compound solubility in aqueous assay buffer (Table 1). Compounds **21** and **23**, with improved solubility, enhanced the basal PKG1α activity with an estimated EC_{50} of ~ 78 μM for **23** while 32% PKG1α activation was observed in the presence of 200 μM of **21** (Fig. 3B and Table 1). These piperidine series activators also enhanced the activity of PKG1α partially activated by cAMP (1 μM cAMP $\sim EC_{20}$) with similar potencies (Fig. 3C).

Validation of direct target engagement

Direct binding of these compounds to PKG1α was confirmed using microscale thermophoresis (MST) and saturation transfer difference (STD) NMR spectroscopy. Figure 4A shows changes in thermophoresis of partially activated PKG1α (with 10 nM cGMP) in the presence of increasing concentrations of compound **1**, **2**, or **21**, indicating direct binding by each compound. The concentration–response curves allowed a K_d estimate for compound **21** of ~ 16 μM while limitations in the soluble concentration range prevented estimates of K_d values for **1** and **2** (Table 1). ^{1}H STD NMR spectroscopy was used as an orthogonal method to validate direct target engagement of the piperidine series activators. In this technique, ^{1}H NMR spectra are acquired on samples that are mixtures of small molecules and proteins. STD NMR spectra show specific ligand protons that are affected by radio frequency saturation that is transferred from the protein to the ligand during binding. After becoming saturated, weak binding ligands dissociate from the protein and are detected free in solution. Saturation leads to a small decrease in some ligand NMR peaks. Peak intensity changes are identified by collecting reference spectrum (on the same sample with no saturation) that is subtracted from data with saturation, resulting in STD spectra. STD NMR peaks are typically detected for ligand-binding affinities that range from micromolar to millimolar. High-affinity ligands stay bound to the target (slow dissociation) and are not directly detected. Figure 4B shows the results of STD NMR binding studies for **1** and **21** in equilibrium with full-length PKG1α. Weak binding of 100 μM compound **1** to 5 μM apo-PKG1α is confirmed by the presence of ligand STD NMR peaks (*blue*). Addition of 10 μM cGMP does not affect compound binding (*red*), indicating that **1** and cGMP bind to
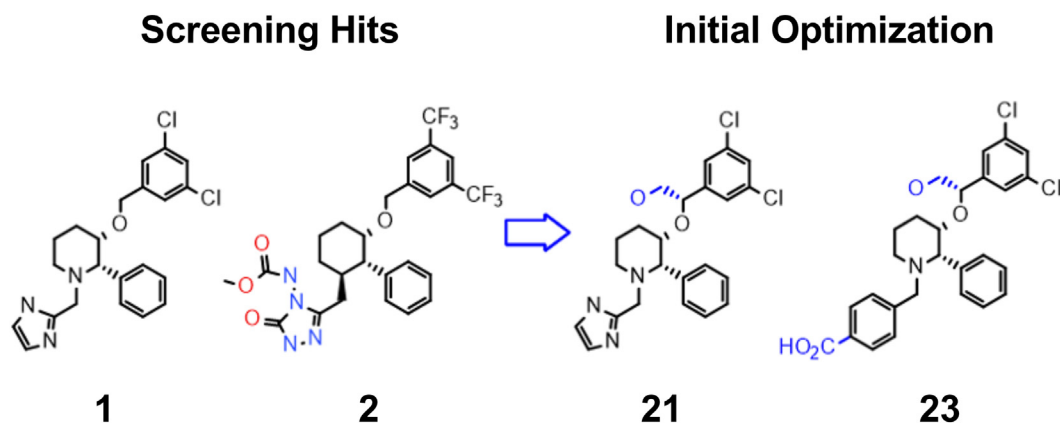
Screening Hits

Initial Optimization

Figure 2. Structure of small molecule activators of PKG1α. Compounds **1** and **2** were original hits identified from compound library screen; compounds **21** and **23** were synthesized from initial optimization of piperidine **1** (23). PKG, cGMP-dependent protein kinase.

different sites. Weak binding of 100 μM compound **21** to 5 μM of apo-PKG1α is confirmed by the presence of ligand STD NMR peaks (*blue*). Addition of 5 μM and 50 μM cGMP does not affect **21** binding (*red* and *black*, respectively), indicating that **21** and cGMP bind to different sites. STD NMR binding studies confirmed **1** and **21** binding to full-length PKG1α. K_d values were not derived from this data.

Piperidine series activators modulate the steady-state kinetic parameters of partially activated PKG1α similar to the modulatory effects of endogenous cGMP

To gain insights to the mechanism of activation of the piperidine series, we first looked at the effect of these compounds on the kinetic parameters of partially activated PKG1α using a microfluidic mobility shift assay (MMSA, see Experimental procedures). Compounds **1**, **2**, and **21** were observed to decrease the K_M of peptide substrate (Glasstide) for PKG1α in a concentration-dependent manner without significant modulation of the catalytic efficiency, k_{cat}, (Fig. 5A). The apparent K_M and k_{cat} for ATP, on the other hand, increased in the presence of compounds **1**, **2**, and **21** (Fig. 5B). The same modulations of enzyme kinetic parameters were observed in the cGMP-induced activation of PKG1α. A 5-fold decrease in peptide K_M with no significant change in k_{cat} was

observed when PKG1α was taken from partially activated state (10 nM cGMP; ~ EC_{20}) to fully activated state (10 μM cGMP; EC_{100}) (Table S1). In the case of ATP, a 3-fold increase in apparent K_M for ATP was observed accompanied by an increase in k_{cat} as PKG1α was taken from partially activated state to the fully activated state (Table S1).

Mutual modulation of binding affinities for PKG1α between piperidine series activators and cGMP

The activity of the original screen hits was observed only for the partially activated PKG1α. This raised the possibility of a binding cooperativity between the piperidine series and cGMP. To evaluate this possibility, we first looked at the effect of the piperidine series on the cGMP-induced activation of PKG1α by tracking the modulation of cGMP EC_{50} in the presence of increasing concentration of piperidines using MMSA method. As shown in Figure 6A, the EC_{50} of cGMP was positively modulated in the presence of increasing concentrations of **21** with a maximal increase in cGMP potency (16-fold decrease in EC_{50}) in the presence of saturating concentrations of **21**. The concentration–response curves ([cGMP] *versus* kinase activity) also showed enhancement of basal activity of PKG1α in the presence of increasing concentrations of **21**, reflecting an ability to activate PKG1α in the absence of cGMP. The same
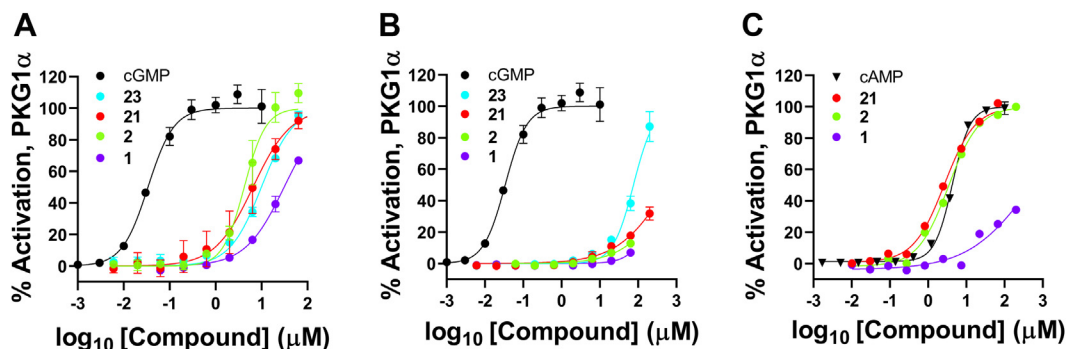

Figure 3. Enhancement of PKG1α activity at increasing concentrations of small molecule activators. *A*, activity of partially activated PKG1α (~EC_{20} with 10 nM cGMP). *B*, basal PKG1α (no cGMP) at increasing concentrations of cGMP, **1**, **2**, **21**, and **23** tracked using ADP-Glo kinase assay. *C*, activity of partially activated PKG1α (~EC_{20} with 1 μM cAMP) at increasing concentrations of cAMP, **1**, **2**, and **21** tracked using HTRF kinase assay. Error bars indicate SE from 2 to 3 independent trials. PKG, cGMP-dependent protein kinase.

Table 1
Potency (EC_{50}) of small molecule activators

| Activator | EC_{50} (μM)[a], PKG1α activation | | | | Solubility[d] (μM) |
| | Kinase assay (ADP-Glo) | | Kinase assay (HTRF) | | |
	No cGMP (basal)	10 nM cGMP ($\sim EC_{20}$)	No cGMP (basal)	10 nM cGMP ($\sim EC_{20}$)	
1	>67	47.2 ± 0.3	>67	45 ± 5	63
2	>67	5 ± 1	>67	5 ± 1	63
21	32 ± 4%[b]	7 ± 4	40 ± 10%[b]	6 ± 1	200
23	80 ± 10	11 ± 1	NT[c]	NT	200

Abbreviation: HTRF, homogeneous time resolved fluorescence.
[a] EC_{50} values were average of 2 to 3 independent trials (errors represented as ± SE).
[b] Percent activation of PKG1α at 200 μM compound concentration.
[c] Not tested.
[d] In assay buffer.

positive modulation of cGMP EC_{50} was also observed in the presence of other members of the piperidine series (Fig. S1). We next evaluated the effect of cGMP on the binding affinity of piperidine series for PKG1α using MST. As shown in Figure 6B, an almost 9-fold enhancement in binding affinity of **21** for PKG1α (decrease in apparent K_d from ~14 μM down to ~1.6 μM) was observed as cGMP was increased from 10 nM to 100 nM. Overall, our results were consistent with mutual positive allosteric modulation of binding affinities for full-length PKG1α between piperidine series activators and cGMP.

Piperidine series are allosteric activators that positively modulate cGMP affinity for CNB-A and negatively modulate cGMP affinity for CNB-B

To determine the localization of piperidine series binding site relative to CNB-A and CNB-B, we evaluated the modulation of apparent affinity ($K_{d, app}$) of cGMP for each site in the presence of increasing concentrations of piperidine series activator. A linear relationship between cGMP $K_{d, app}$ values with increasing concentration of small molecule activator will indicate direct binding competition for the same CNB site. On the other hand, a curvilinear relationship between cGMP $K_{d, app}$ with increasing small molecule activator concentration will indicate allosteric modulation of cGMP binding affinity and the existence of a unique piperidine series binding site

allosteric from the cGMP-binding site. We used fluorescently labeled cGMP, 8-fluo-cGMP, to probe the modulation of cGMP binding affinity for CNB sites in the presence of small molecule activator. Fluorescence polarization (FP) method was used to monitor binding of 8-fluo-cGMP to PKG1α. In this method, the FP signal of 8-fluo-cGMP increases as a result of a change in its rotation speed in solution: from a fast rotation when free in solution to a much slower solution rotation speed when bound to PKG1α. The increase in FP signal is proportional to the fraction of 8-fluo-cGMP bound to PKG1α.

To evaluate modulation of cGMP affinity for CNB-A, a FP binding assay was performed to track binding of 8-fluo-cGMP to CNB-A site in full-length PKG1α. At conditions where only CNB-A was populated by 8-fluo-cGMP (10 nM PKG1α and 0.5 nM 8-fluo-cGMP, see Experimental procedures for details), an increase in the fraction of 8-fluo-cGMP bound to PKG1α was observed in the presence of increasing concentrations of **21** or **23** (increase in FP signal, Fig. 7Aa). This indication of enhanced affinity for CNB-A in the presence of piperidines directly contrasted with a decrease in fraction of 8-fluo-cGMP bound to PKG1α (decrease in FP signal) in the presence of increasing concentrations of an orthosteric competitor such as unlabeled cGMP, 8Br-cGMP, or cAMP (Fig. 7Aa). To further clarify the observed positive modulation of cGMP affinity for CNB-A by piperidines, we measured the apparent affinity of 8-fluo-cGMP (FP of 8-fluo-cGMP [0.5 nM] with titration of
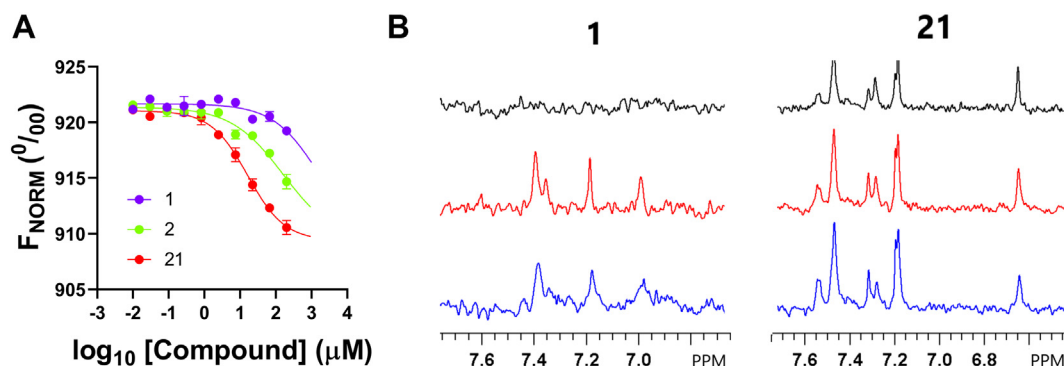

Figure 4. Validation of direct target engagement of piperidine series. *A*, changes in thermophoresis of partially activated PKG1α (with 10 nM cGMP) upon binding of small molecule activators. Concentration–response curves were shown for **1**, **2**, and **21**. K_d for **21** was estimated at ~16 ± 4 μM (Mean ± SE; n = 2). K_d estimates for **1** and **2** was not possible due to limitations in solubility. *B*, direct binding of piperidines to PKG1α monitored by ^{1}H STD NMR. *Left panel*: binding of **1** to apo-PKG1α led to observed peaks in the STD NMR spectrum (*blue*); compound **1** binding was not affected by the addition of 10 μM cGMP (*red*). A control spectrum with **1** and no protein shows no peaks (*black*). *Right panel*: binding of **21** to apo-PKG1α (*blue*) was not affected by the addition of 5 and 50 μM cGMP (*red* and *black*, respectively). PKG, cGMP-dependent protein kinase; STD, saturation transfer difference.
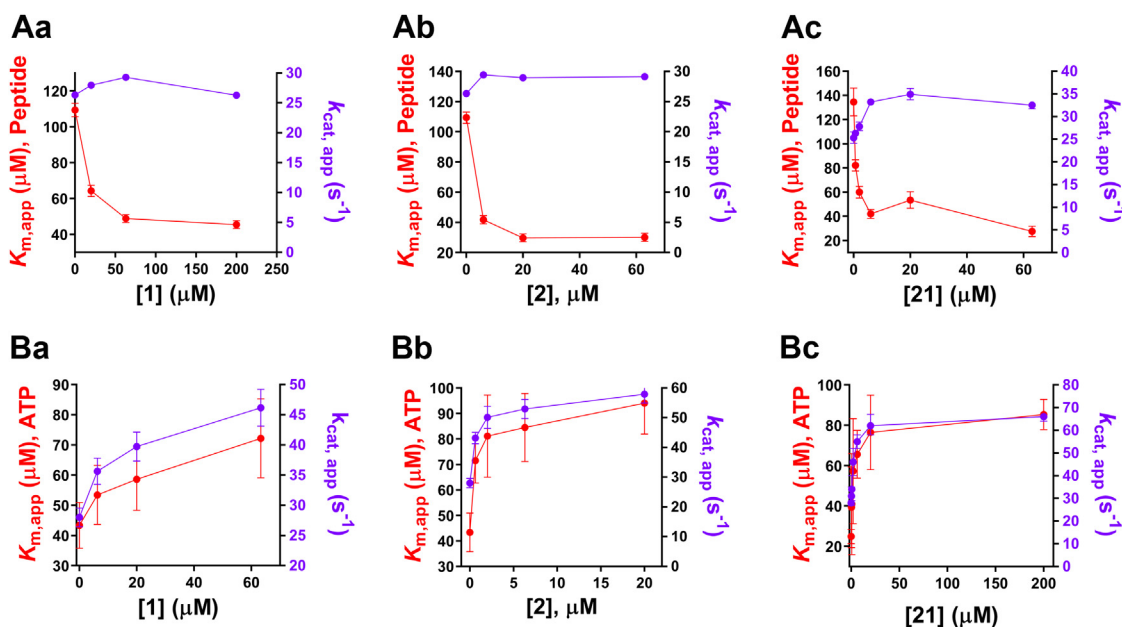
Figure 5. Modulation of kinetic parameters of partially activated PKG1α by small molecule activators. *A*, positive modulation of peptide substrate K_M (*red*) with no significant change in k_{cat} (*purple*) in the presence of (*Aa*) **1**, (*Ab*) **2**, or (*Ac*) **21**. *B*, negative modulation of apparent K_M (*red*) for ATP with increase in k_{cat} (*purple*) in the presence of (*Ba*) **1**, (*Bb*) **2**, or (*Bc*) **21**. Error bars indicate 95% confidence interval from nonlinear regression fits used to estimate kinetic parameters. PKG, cGMP-dependent protein kinase.

PKG1α) in the presence of increasing concentrations of piperidines. As shown in Figure 7*A*b, an increase in apparent affinity of 8-fluo-cGMP for CNB-A with increasing concentration of **23** was clearly observed in the left shift trend of the concentration–response curves. The apparent K_d values for best fit curves plotted against concentration of **23** revealed a curvilinear relationship, indicating piperidines allosterically enhance the affinity of cGMP for CNB-A (Fig. 7*A*c). At saturating concentrations of **23**, we observed an almost 4-fold enhancement of affinity of 8-fluo-cGMP for CNB-A.

We next determined the modulatory effect of piperidines on cGMP affinity for CNB-B. We first set up a FP binding assay at

conditions where 8-fluo-cGMP occupied both CNB-A and CNB-B (100 nM PKG1α in equilibrium with 200 nM 8-fluo-cGMP). As shown in Figure 7*Ba*, a partial decrease in the fraction of 8-fluo-cGMP bound to PKG1α was observed (a partial decrease in FP signal) in the presence of increasing concentrations of either **21** or **23**. This indicated piperidines compete with cGMP for the CNB-B site as CNB-A site remained occupied by 8-fluo-cGMP. To further highlight these observations, we used unlabeled cGMP as surrogate for a direct (orthosteric) competitor for both the CNB-A and CNB-B sites. As shown in Figure 7*Ba*, increasing concentrations of unlabeled cGMP decreased the FP signal down to background
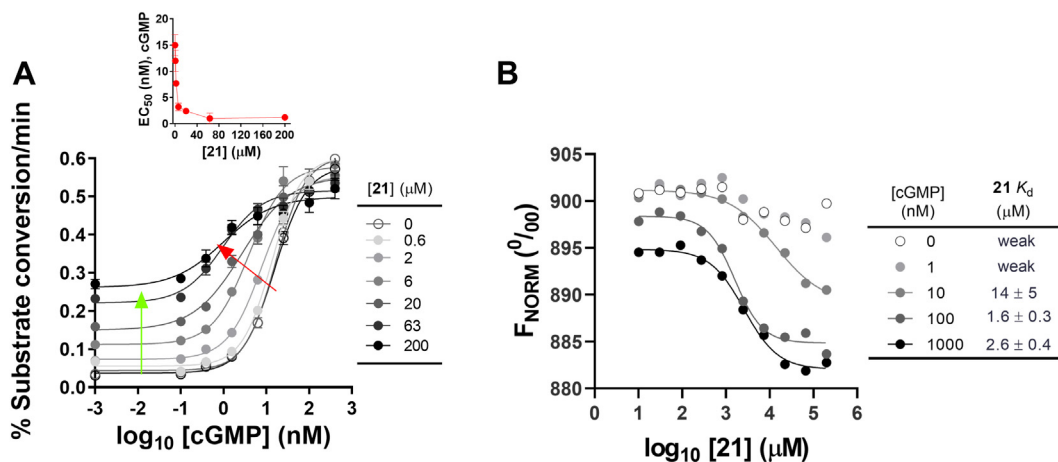

Figure 6. Mutual positive modulation of affinity for PKG1α between piperidine series activators and cGMP. *A*, cGMP EC_{50} estimates in the presence of increasing concentrations of compound **21**. The *red arrow* indicate left shift of the concentration–response curves (decrease in cGMP EC_{50}) in the presence of increasing concentrations of **21**; *green arrow* indicate increase in basal activity (no cGMP) in the presence of increasing concentrations of **21**. Inset graph shows cGMP EC_{50} values for best fit curves plotted against concentration of **21** (error bars indicate SE from two independent trials). PKG1α activity (initial velocities) were measured using microfluidic mobility shift assay. *B*, increase in binding affinity of **21** for PKG1α in the presence of increasing concentrations of cGMP. Binding affinities (K_d) were estimated by measuring changes in thermophoresis of PKG1α in the presence of varying concentrations of cGMP. Error (±SE) represents the standard error of nonlinear least squares regression. PKG, cGMP-dependent protein kinase; SE, standard error.
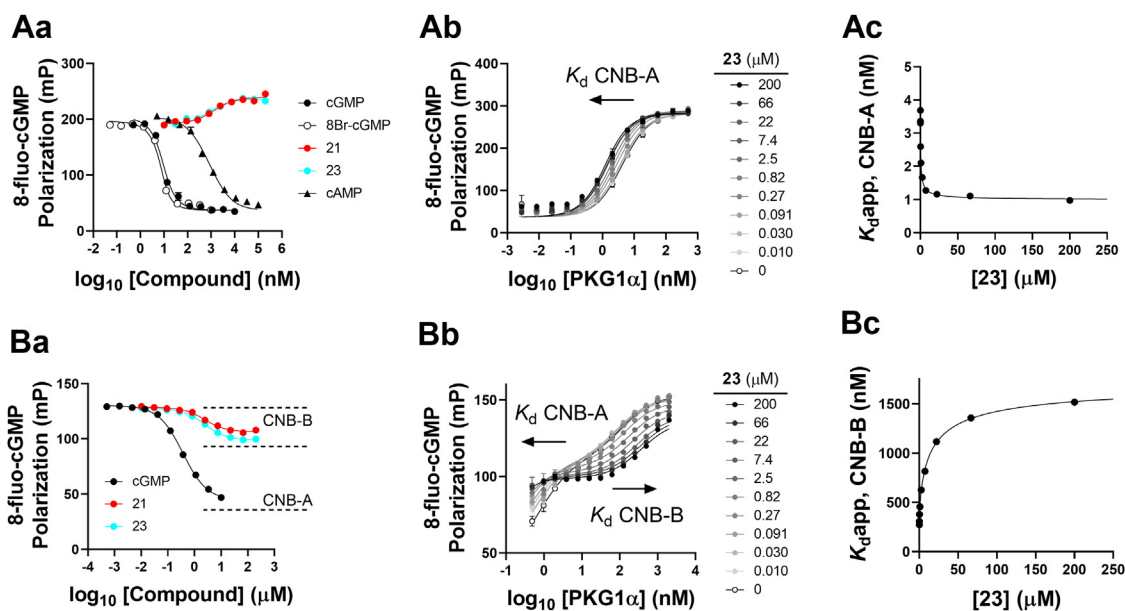
Figure 7. Fluorescence polarization assays measuring effect of piperidines on cGMP binding to CNB-A and CNB-B in full-length PKG1α (PKG1α$_{2-671}$). *A*, enhancement of 8-fluo-cGMP binding affinity for CNB-A. *Aa*, Increase in fraction of 8-fluo-cGMP bound to full-length PKG1α (increase in polarization signal) with increasing concentrations of **21** and **23**. In contrast, a decrease in polarization was observed in the presence of increasing concentration of direct competitors (unlabeled cGMP, 8Br-cGMP, and cAMP). *Ab*, 8-fluo-cGMP affinity estimates. The increase in apparent affinity of 8-fluo-cGMP for CNB-A site with increasing concentration of **23** observed in the left shift trend of the concentration response curves. Error bars represent SE from two replicate measurements. *Ac*, Curvilinear relationship between affinity of 8-fluo-cGMP for CNB-A and concentration of **23** indicating piperidines bind to a site allosteric to CNB-A (K_d for best fit curves from panel *Ab*). *B*, negative modulation of cGMP affinity for CNB-B. *Ba*, At conditions where both CNB-A and CNB-B were populated by 8-fluo-cGMP, a partial decrease in fraction of 8-fluo-cGMP bound to PKG1α (decrease in polarization signal) was observed in the presence of increasing concentrations of **21** and **23**, indicating competition for CNB-B as 8-fluo-cGMP remained bound to CNB-A. In contrast, unlabeled cGMP decreased polarization signal to baseline level indicating direct competition for both CNB-A and CNB-B sites. *Bb*, Sequential two-site equilibrium binding of 8-fluo-cGMP to PKG1α. A decrease in apparent affinity of 8-fluo-cGMP for CNB-B with increasing concentration of **23** observed as a right shift in the portion of the concentration–response curve corresponding to binding to CNB-B. Error bars represent SE from two replicate measurements. *Bc*, Curvilinear relationship between apparent 8-fluo-cGMP K_d and concentration of **23** indicating piperidines bind to a site allosteric to CNB-B. CNB, cyclic nucleotide binding domain; PKG, cGMP-dependent protein kinase; SE, standard error.

levels indicating complete displacement of 8-fluo-cGMP from both CNB-A and CNB-B sites as expected for orthosteric competition.

The indication that the piperidine series competes for the low affinity cGMP-binding site prompted further studies to elucidate whether these activators bind directly to CNB-B (orthosteric competition) or to a unique site allosteric to CNB-B (allosteric competition). To distinguish between these two modes of competitive binding, we set out to determine the modulation of apparent affinity ($K_{d, app}$) of cGMP for CNB-B site in the presence of increasing concentration of piperidine series activator. To enable measurement of cGMP binding affinity for CNB-B, a novel two-site FP binding assay was configured based on a sequential two-site equilibrium binding model where K_d1 and K_d2 are the cGMP binding affinities for the CNB-A and CNB-B site, respectively.

$$P + cGMP \overset{K_d1}{\leftrightarrow} P(cGMP) + cGMP \overset{K_d2}{\leftrightarrow} P(cGMP)_2$$
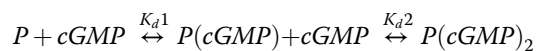
Starting at a condition where the two CNB sites are fully occupied at a 1:2 molar ratio of PKG1α and 8-fluo-cGMP (at concentrations well above the K_d values for the two CNB sites), PKG1α and 8-fluo-cGMP concentrations were then varied in a dilution series while maintaining the 1:2 protein to 8-fluo-cGMP ratio (see Experimental procedures for details). The observed FP signal from the resulting solutions tracked the

equilibrium titration of 8-fluo-cGMP across the two CNB sites: binding first to the high affinity CNB-A site, then to the low affinity CNB-B site, as the concentrations of both PKG1α and 8-fluo-cGMP increase. The plot of FP (∼fraction of 8-fluo-cGMP bound to PKG1α) *versus* PKG1α concentration was fitted to a sequential two-site binding equation (Equation 9 in Experimental procedures) to estimate cGMP affinities for both CNB sites (K_d1 and K_d2). The estimated 8-fluo-cGMP K_d for CNB-A and CNB-B using this method closely matched the corresponding cGMP K_d estimates using isothermal titration calorimetry method (Fig. S2C) confirming the robustness of the assay and validate the use of 8-fluo-cGMP as a surrogate for cGMP. We then determined the apparent K_d of 8-fluo-cGMP at both sites in the presence of increasing concentrations of small molecule activator. As shown in Figure 7Bb, although the assay in this format is not sensitive enough to deconvolute the apparent K_d of 8-fluo-cGMP for CNB-A below 2 nM, the positive allosteric modulation of cGMP affinity for CNB-A at increasing concentration of **23** can still be observed as a left shift in the segment of the concentration–response curve corresponding to 8-fluo-cGMP binding to CNB-A. On the other hand, the affinity of 8-fluo-cGMP for CNB-B site was clearly shown to decrease with increasing concentration of **23** as observed in the right shift of the concentration–response curves corresponding to binding to CNB-B (Fig. 7Bb). An almost 6-fold increase in apparent 8-

fluo-cGMP K_d (decrease in apparent affinity) for CNB-B was observed in the presence of saturating concentration of **23** (from 280 nM to ~1700 nM $K_{d, \text{app}}$; Fig. 7*Bc*). The curvilinear relationship between apparent 8-fluo-cGMP K_d and concentration of **23** (Fig. 7*Bc*) indicated allosteric competition for CNB-B. To provide contrast and further highlight this observation, we also determined the relationship between the apparent affinity of 8-fluo-cGMP and concentration of orthosteric competitors (unlabeled cGMP and cAMP) using the same two-site binding assay. The presence of increasing concentrations of each of these direct competitors decreased the apparent affinity of 8-fluo-cGMP for the two binding sites as indicated by rightward shift of the concentration–response curves (Fig. S3, *Aa* and *Ba*). A plot of apparent K_d of 8-fluo-cGMP for CNB-A and concentration of cGMP (Fig. S3*A*b) or cAMP (Fig. S3*B*b) showed a linear relationship, indicating direct competition for the same binding site.

Piperidine series allosteric binding site is in the regulatory domain

To confirm the binding localization of the piperidine series and to gain additional insights to mechanism of action, we evaluated the modulation of cGMP binding affinity for the isolated regulatory domain fragment (CNB sites and switch helix; PKG1α$_{79-356}$) in the presence of piperidine series activator. To evaluate the modulation of cGMP binding to CNB-A, we measured the apparent affinity of 8-fluo-cGMP (polarization of 8-fluo-cGMP [0.5 nM] with titration of PKG1α$_{79-356}$) in the presence of increasing concentration of **23**. As shown in Figure 8, *Aa* and *Bb*), no significant shift in the concentration–response curves (and corresponding estimates of apparent 8-fluo-cGMP K_d) was observed at increasing concentration of **23** (up to saturating level ~200 μM).

To evaluate the effect of piperidines on cGMP binding to CNB-B in PKG1α$_{79-356}$, the FP two-site binding assay was performed to estimate the apparent K_d of 8-fluo-cGMP for CNB-B, applying similar conditions used for the full-length protein. As shown in Figure 8*Ba*, a decrease in apparent affinity of 8-fluo-cGMP for CNB-B with increasing concentration of **23** was observed as a right shift in the portion of the concentration–response curve corresponding to binding to the low affinity site indicating a negative modulation of 8-fluo-cGMP affinity. The plot of apparent K_d against the concentration of **23** showed a curvilinear relationship (Fig. 8*Bb*), confirming the allosteric localization of piperidine series binding site within the regulatory domain.

A competition binding analysis using ^{1}H STD NMR was also performed to confirm allosteric binding of piperidine series to PKG1α$_{79-356}$. A solution containing **1** and cAMP in
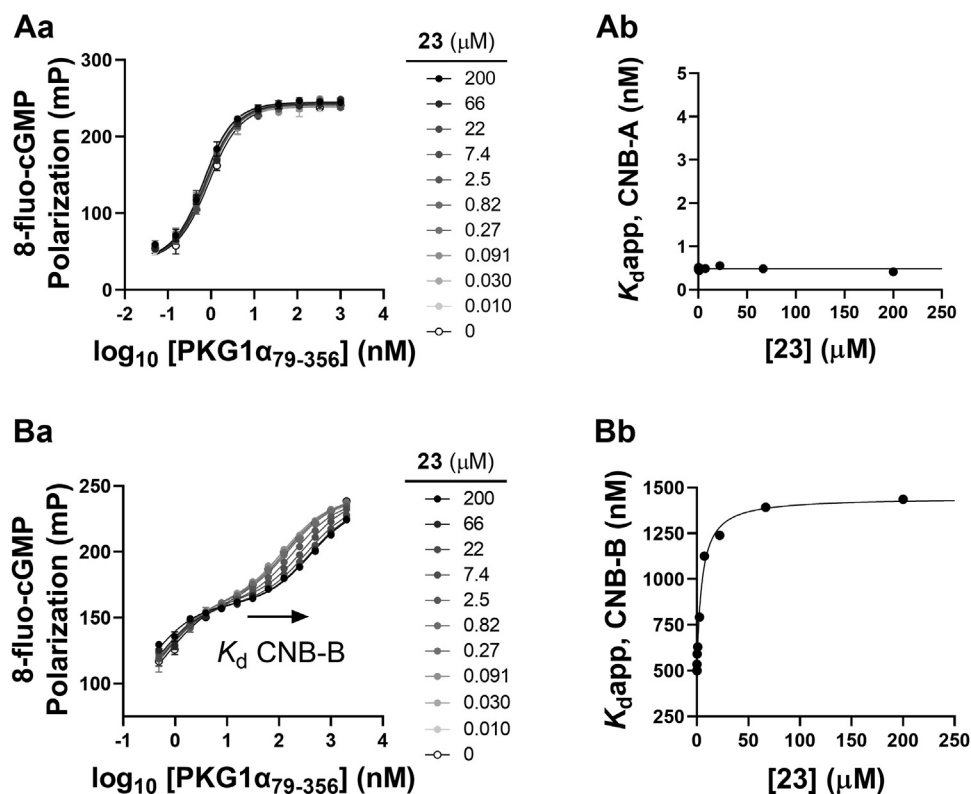

Figure 8. Fluorescence polarization assays measuring effect of piperidines on cGMP binding affinity for CNB-A and CNB-B in regulatory domain, PKG1α$_{79-356}$. *A*, effect of piperidines on 8-fluo-cGMP binding to CNB-A. *Aa*, 8-fluo-cGMP affinity estimates (polarization of 8-fluo-cGMP (0.5 nM) with titration of PKG1α$_{79-356}$). The presence of compound **23**, up to 200 μM, had no effect on the concentration–response curve. Error bars represent SE from two replicate measurements. *Ab*, No significant modulation of 8-fluo-cGMP affinity with increasing concentration of **23** (K_d values for best fit curves from Panel *Aa*). *B*, effect of piperidines on cGMP binding to CNB-B. *Ba*, Sequential two-site equilibrium binding of 8-fluo-cGMP to PKG1α$_{79-356}$. A decrease in apparent affinity of 8-fluo-cGMP for CNB-B with increasing concentration of **23** was observed as a right shift in the portion of the dose–response curve corresponding to the low affinity site, CNB-B. *Bb*, Curvilinear relationship between 8-fluo-cGMP K_d *versus* compound **23** concentration supported allosteric localization of piperidine series binding site to the regulatory domain, PKG1α$_{79-356}$. CNB, cyclic nucleotide binding domain; PKG, cGMP-dependent protein kinase.

equilibrium with PKG1α$_{79-356}$ showed signature peaks from both **1** and cAMP in the STD NMR spectrum indicating binding of **1** and cAMP to different sites in PKG1α$_{79-356}$ (Fig. S4*B*). In contrast to this observation, addition of a saturating concentration of cGMP to a solution containing cAMP in equilibrium with PKG1α$_{79-356}$ resulted in the disappearance of the cAMP peaks in the STD NMR spectrum (Fig. S4*A*), indicating direct competition for the same binding sites. Note that cGMP signal is not observable in STD NMR due to its relatively high affinity to CNB-A and CNB-B (Fig. S2*C*).

In silico *modeling studies identified a possible piperidine series interaction site near CNB-B*

To further investigate the potential binding site for small molecule activators, an *in silico* model was built based on the previously published 3SHR (17) structure of the regulatory domain, PKG1α $_{78-355}$ (Figs. 9 and 10*A*). Within this structure, the monomer was probed for potential binding sites. The five largest sites identified were examined. Sites *S1* and S2, the two largest sites, were of similar size and corresponded to the cGMP-binding pockets. Site *S3* was highly surface exposed and did not yield any significant interactions on binding. Site *S5* was eliminated as it occurs at the N terminus of the sequence

Figure 9. *In silico* **modeling study to identify possible small molecule binding site based on 3SHR** (17) **structure of PKG1α** $_{78-355}$**.** Largest sites as identified by the site finder algorithm: *S1* and *S2* correspond to cGMP low affinity and high affinity binding sites, respectively. *S3* is a large shallow, mostly hydrophilic site with significant solvent exposure. *S5* is located at the N terminus in the truncated region of the sequence. *S4* is a large hydrophobic site that was considered to be the most likely binding site for the allosteric interaction site. The sites are rendered with mesh surfaces colored by lipophilicity. PKG, cGMP-dependent protein kinase.

of 3SHR and is a possible artifact of truncation (Fig. 9). Site *S4* appeared to be the most interesting consisting of a mostly hydrophobic pocket within the regulatory domain, proximal to CNB-B. While docking of the small molecule activator, **23**, was attempted at all sites, the *Site 4* pocket demonstrated excellent shape complementarity with significant arene-π interactions occurring throughout the pocket (Fig. 10, *B* and *C*). This pocket is occupied by Phe$_{350,351}$ and Leu$_{354}$ of the opposite chain switch helix in the full structure (17). The molecule mimicked the insertion of Phe$_{350,351}$ and Leu$_{354}$ (Fig. 11). A search for potential alternate binding sites, including the cGMP-binding pockets themselves, did not identify a region more compatible than that observed at the identified allosteric pocket.

Discussion

As the major effector of the beneficial effects of cGMP signaling, PKG1 represents a compelling drug target for treatment of cardiovascular diseases. Current therapeutic agents that modulate the cGMP signaling pathway work by increasing cGMP levels and subsequent activation of PKG1. Direct pharmacological activation of PKG1, independent of cGMP, presents an attractive route to gain additional efficacy as this may capture the benefits of cGMP-PKG signaling while avoiding the possible complicating effects of multiple downstream signaling pathways also activated by cGMP. To search for small molecule activators of PKG1α, we screened a diverse library of ∼2.9 million compounds against the basal and partially active enzyme (23). The inclusion of the partially activated state in the uHTS screen was based on its likely relevance *in vivo* due to the known high affinity of cGMP and cAMP for CNB-A (17) and the basal tone of these endogenous activators in the cell (24) that can favor partial activation of PKG1α. Here, we describe the characterization of a piperidine series of activators, initially identified from uHTS screen (Fig. 2), as part of a larger drug discovery effort focused on direct activation of PKG1α.

The uHTS hits, **1** and **2**, and synthesized compounds from initial optimization efforts, **21** and **23**, enhance the kinase activity of partially activated PKG1α (∼EC$_{20}$ with 10 nM cGMP or 1 μM cAMP) in a concentration-dependent manner (Fig. 3, *A* and *C*). The observed ability of these compounds to enhance activity of PKG1α partially activated by cAMP may have added significance as cAMP may partially (cross-) activate PKG1α in the background of very low cGMP concentration in the disease state. Initial optimization of the original screen hit, **1**, resulted in an immediate 4- to 7-fold improvement in EC$_{50}$ for analogs **21** and **23** on the partially activated enzyme (Table 1). More importantly, these piperidine analogs have an ability to enhance the activity of PKG1α from the basal state, independent of cGMP (Figs. 3*B*, 6*A*, and Table 1). A detailed exploration of structure activity relationships revealed the addition of a hydroxy methyl group in **23** is responsible for improved activity relative to the parent piperidine **1** (23). Additionally, the combination of a carboxylic acid and the hydroxy methyl group were identified as modifications that
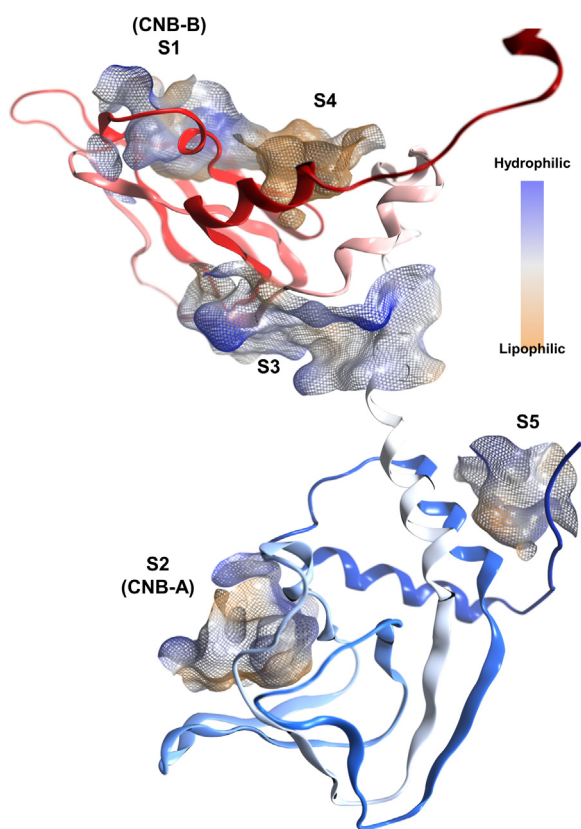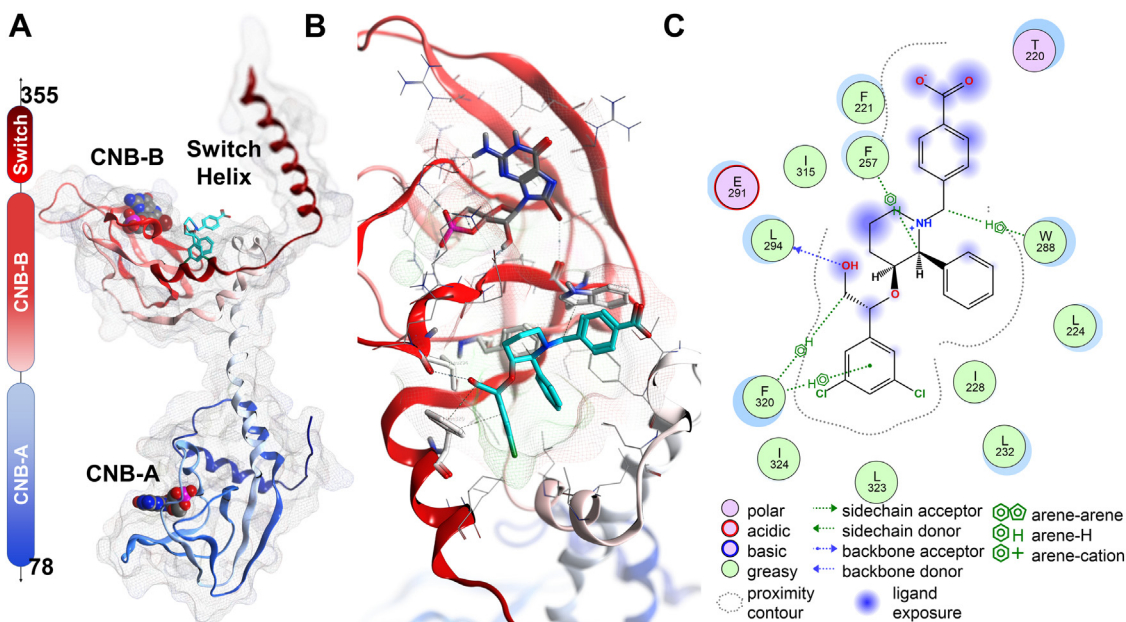
Figure 10. *In silico model of possible allosteric interaction site within PKG1α $_{78-355}$ based on 3SHR* (17). *A*, cGMP (*gray*-spacefill) is bound at both low and high affinity sites with compound **23** (*cyan sticks*) bound proximal to the low affinity cGMP site at CNB-B. *B*, a distinct pocket is observed with shape complementarity to the ligand and significant H-π interactions throughout the site as can be observed in the ligand interaction diagram, (*C*). CNB, cyclic nucleotide binding domain; PKG, cGMP-dependent protein kinase.

enhanced the potency of the N-benzyl analog, **23**, relative to the parent piperidine **1**. These modifications likely created affinity-enhancing interactions as indicated by the stronger affinity of **21** for the partially activated PKG1α, relative to the parent piperidine **1** (Fig. 4*A*), with consequent improvement in compound potency. The modifications in **21** and **23** also resulted in relative improvements in solubility (Table 1) and cell permeability (23) enabling analysis of compound activity in the cell. We demonstrated on-target cell-based activity for these small molecules by measuring the PKG1α phosphorylation of the known endogenous substrate, vasodilator-stimulated phosphoprotein (VASP), which gave EC_{50} values
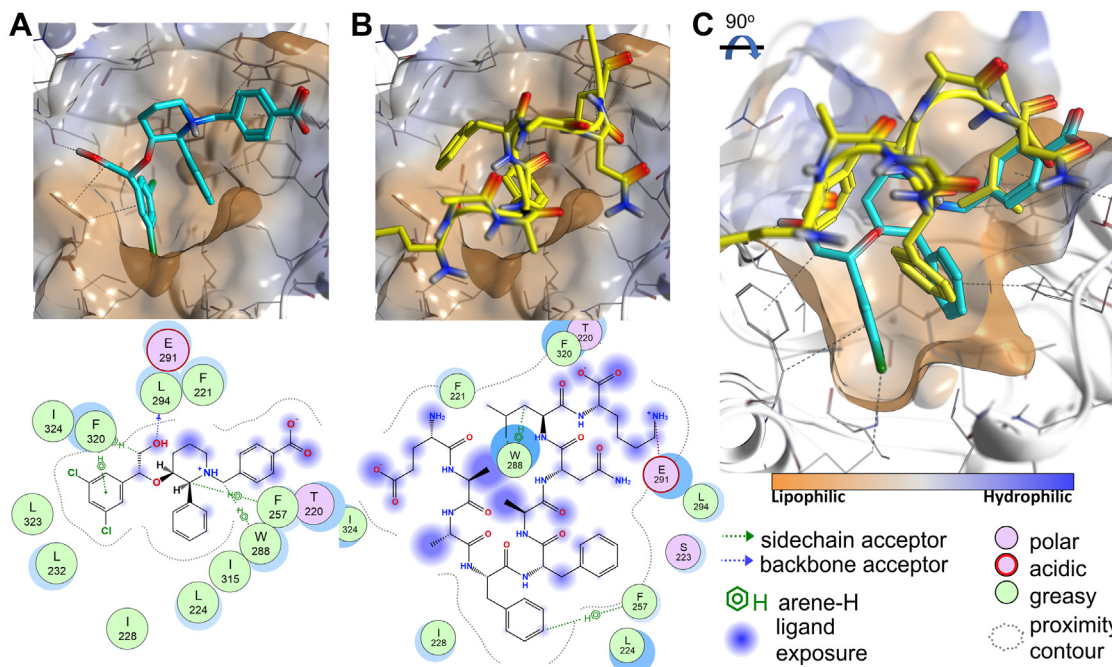

Figure 11. Overlap of possible small molecule–binding site with switch helix interaction site based on 3SHR. *A*, compound **23** (*cyan*) as docked into the hydrophobic nest pocket (*S4*). H-π and H-bonding interactions are observed throughout the pocket and principally occur with Phe$_{257}$ and Trp$_{288}$ among others. These interactions were conserved when compared with the switch helix (*yellow*) (*B*). When viewed from the side cut-away of the pocket (*C*), in the overlay, compound **23** is observed to penetrate deeper into the hydrophobic pocket and displays a larger number of interactions, perhaps explaining its ability to activate PKG1α through displacement of the switch helix. PKG, cGMP-dependent protein kinase.

for **21** and **23** of 9 µM and 15 µM, respectively (23). The observed cell-based activity added critical validation for the piperidine series and their potential for development.

To gain insights to the mechanism of PKG1α activation by the piperidine series, we first looked at how these small molecules modulate the kinetic parameters of PKG1α in comparison to cGMP. The observed increase in peptide substrate affinity (decrease in K_M of Glasstide) in the presence of small molecule activator suggested an enhanced substrate access to the catalytic site (optimized binding mode) favorable for catalysis (Fig. 5A). This positive modulation of peptide substrate affinity, along with the observed increase in apparent K_M for ATP (with increase in k_{cat}) at increasing small molecule concentration (Fig. 5B), demonstrated an overall similarity to modulations in enzyme kinetic parameters observed in the cGMP-induced activation of PKG1α (Table S1 and published reports (15, 25–27)). These observations indicate that the piperidine series activators elicit the same mechanisms associated with cGMP-induced activation of full-length PKG1α.

With the observed similarity in modulating enzyme kinetic parameters between piperidine series activators and cGMP, we set out to clarify whether these small molecules are cGMP mimetics and bind to one of the CNB sites. Direct binding to full-length enzyme was demonstrated in the presence and absence of cGMP (Fig. 4, A and B). The binding of these small molecules to PKG1α in the presence of cGMP (Fig. 4B) was an early indication of the existence of a piperidine series binding site allosteric to one or both CNB sites. This aligned with our earlier observation that the uHTS hits (**1** and **2**) enhanced activity of partially activated PKG1α (Fig. 3, A and C) but not the basal state (Fig. 3B). Indeed, results consistent with mutual positive allosteric modulation of affinities for full-length PKG1α were observed between piperidines and cGMP supporting the existence of an allosteric binding site for these small molecule activators (Figs. 6 and S1).

To establish the localization of the piperidine series binding site relative to CNB-A and CNB-B, we used FP-based equilibrium binding assays to determine the effect of small molecule activator on the cGMP-binding affinity for each CNB site in full-length PKG1α. A linear relationship between the apparent affinity of labeled cGMP (8-fluo-cGMP) and small molecule concentration would indicate direct (orthosteric) competition for the same binding site, while a curvilinear relationship between 8-fluo-cGMP apparent affinity and small molecule concentration will indicate allosteric binding relative to the cGMP binding site in full-length PKG1α. Because the uHTS hits only enhance the activity of partially activated PKG1α, we hypothesized that the piperidines likely do not bind to CNB-A which should be populated by cGMP in the partially activated enzyme. This was validated by observations of enhanced 8-fluo-cGMP affinity for CNB-A in full-length PKG1α at increasing concentrations of piperidine series activator (Fig. 7A). The curvilinear relationship between apparent 8-fluo-cGMP K_d for CNB-A and small molecule concentration validated the allosteric localization of the piperidine series binding site relative to CNB-A (Fig. 7Ac). The observed allosteric enhancement of 8-fluo-cGMP affinity for CNB-A in the

presence of small molecule activator was consistent with earlier observations of mutual positive modulation of binding affinity for PKG1α between cGMP and piperidine series (Figs. 6 and S1).

In the case of CNB-B site, initial competition binding analysis indicated the piperidines compete with cGMP for the CNB-B site (Fig. 7Ba). We further evaluated the nature of this competition binding (orthosteric *versus* allosteric competition) to determine the localization of the piperidine series binding site relative to CNB-B. A novel FP-based two-site binding assay allowed the specific measurement of cGMP binding affinity for CNB-A and CNB-B. We observed a negative modulation of 8-fluo-cGMP binding affinity for CNB-B in the presence of increasing concentration of small molecule activator (Fig. 7, Bb and Bc). The curvilinear relationship between the apparent 8-fluo-cGMP K_d and small molecule concentration indicated allosteric competition and the existence of a small molecule binding site distinct from CNB-B. This observation of negative binding cooperativity between small molecule binding site and CNB-B support a mechanism of small molecule–induced PKG1α activation that do not involve binding to CNB-B. We note that in the case of the cGMP-induced PKG1α activation, a negative binding cooperativity between cGMP-binding sites, CNB-A and CNB-B, was demonstrated (14). Assessment of the contribution of each of the CNB sites to enzyme activation led to the conclusion that CNB-B site has a nonessential role in cGMP-induced kinase activity (14). Using site-directed mutagenesis to disrupt binding of cGMP to each of the CNB site, Moon *et al.* showed that only the disruption of cGMP binding to CNB-A resulted in abolishing activation of kinase activity (14).

We narrowed down the localization of the piperidine series binding site within the regulatory domain fragment, PKG1α$_{79-356}$, encompassing the cyclic nucleotide-binding sites and the switch helix (see Fig. 1). A competition binding analysis, monitored by ^{1}H STD NMR, showed signals from both piperidine series activator and cAMP in the STD NMR spectrum supporting the existence of a small molecule–binding site unique from the CNB sites within the isolated PKG1α$_{79-356}$ (Fig. S4B).

To gain further insights to the mechanism of action of these small molecule activators, we evaluated the modulation of cGMP affinity for CNB-A and CNB-B by small molecule activator in the context of the isolated regulatory domain fragment (PKG1α$_{79-356}$) using the same FP-based binding studies performed on full-length enzyme. The positive binding cooperativity observed between CNB-A and piperidine-binding site in the full-length enzyme, PKG1α$_{2-671}$ (Fig. 7A), was not preserved in the isolated PKG1α$_{79-356}$ (Fig. 8A). This indicated that the positive cooperativity between CNB-A and small molecule activator binding site was likely facilitated by mechanisms that exist in the environment of the full-length enzyme. The importance of the full-length protein environment was also demonstrated for the observed positive cooperativity in the cGMP-induced activation of full-length PKG1α (13, 27). This positive cooperativity was not observed in the truncated enzyme missing the dimerization domain

(monomeric PKG1α $_{78-671}$) leading to the proposal that the mechanism driving this enzyme activation cooperativity lies at the interface between protomers in the full-length (homo-dimer) enzyme (14, 28).

The observed negative cooperativity between CNB-B and piperidine series binding site in full-length PKG1α$_{2-671}$ (Fig. 7B) was preserved in the isolated regulatory domain fragment, PKG1α$_{79-356}$ (Fig. 8B). This further validated localization of piperidine series binding site to the regulatory domain and suggests that the small molecule activator binding site is near CNB-B. To further investigate the possible interaction site of piperidines within the regulatory domain, we conducted *in silico* modeling studies based on the previously published structure of the regulatory domain, PKG1α $_{78-355}$ (Fig. 10A) (17). The modeling studies led to the identification of a unique pocket proximal to CNB-B. Docking studies using **23** clearly demonstrated excellent shape complementarity with significant arene-π interactions occurring throughout the pocket (Fig. 10, B and C). The allosteric nature of this potential binding site, its proximity to CNB-B, and the lack of a similar site near CNB-A was consistent with our overall biochemical and biophysical data. Interestingly, this potential small molecule binding pocket is within the 'nest' site proposed as the binding site for the recently reported peptide-based activators derived from the sequence of the switch helix. These peptides were thought to mimic the C-terminal switch helix 'knob' interaction with the 'nest' site adjacent to the cGMP CNB-B site, facilitating a cGMP-independent activation of PKG1α (22). The most potent peptide, S1.5, is a 24-mer (~2695 Da) truncation derivative of the parent switch helix sequence. The potency of this activator ($K_a \sim 3$ μM) has been shown to derive from the preserved peptide helicity and C terminus 'knob' motif (Phe$_{350}$, Phe$_{351}$, Asp$_{353}$, and Leu$_{354}$) (22). Removal or mutation of the 'knob' residues, including the critical Phe$_{350}$ and Phe$_{351}$, abolished peptide activity, suggesting a mechanism of action involving switch helix interactions observed in the crystal structure of PKG1α regulatory domain (22). In the case of the small molecule activator, **23**, the docking model appears to mimic the binding of three 'knob' residues in the switch helix (Phe$_{350}$, Phe$_{351}$, and Leu$_{354}$; Fig. 11). In particular, the dichloro-phenyl moiety corresponds to the positioning of Phe$_{350}$. The small molecule activator penetrates the nest pocket deeper than the switch helix and displays a larger number of interactions (Fig. 11). Modifications on key substituents of the core piperidine ring, including the benzyl ether and dichloro-phenyl ring moieties, rendered compounds inactive, indicating that these substituents are critical for activity (23) and aligns with their possible involvement in binding site interactions as suggested by the docking model. Crystallographic studies on isolated PKG1α fragment that includes CNB-B and switch helix have since confirmed the binding mode predicted by *in silico* studies (29). The overlap of the small molecule–binding site with the switch helix 'knob' binding site suggests an activation mechanism involving disruption of switch helix interactions that regulate full-length PKG1α activity.

In summary, our work focused on elucidating the mechanism of action of small molecule activators in the context of full-length (homodimeric) PKG1α. In the absence of structural information on full-length enzyme, our data clearly demonstrated that the small molecule activator is not a cGMP mimetic. We thus accomplished our main goal of finding a route to directly activate PKG1α that will avoid activation of other signaling pathways dependent on cGMP. The small molecule modulation of enzyme substrate affinities indicates the piperidine compound series elicit similar mechanism of enzyme activation as the endogenous activator, cGMP. The positive modulation of the peptide substrate K_M is direct evidence of a compound-induced open conformation allowing substrate access to the catalytic site. We demonstrated that the small molecule activator increases the affinity of cGMP for the high affinity binding site (CNB-A) and decreases the affinity of cGMP for the low affinity binding site (CNB-B) in the regulatory domain. The mutual enhancement of binding affinity between small molecule activator (bound to the 'nest' pocket near CNB-B) and cGMP (bound to CNB-A) only exists in the context of the full-length protein. This highlights the importance of the protein environment outside the regulatory domain in facilitating the positive cooperativity between the two sites. This binding cooperativity has direct relevance in the disease state where cGMP is low and PKG1α likely is partially activated by either cGMP or cAMP. We speculate that the compound-induced modulation of PKG1α activity may involve disruption of the switch helix 'knob' interactions that regulate kinase activity. How the displacement of the 'knob' from the 'nest' pocket elicits conformational changes leading to the opening of the catalytic domain remains to be uncovered and will benefit from efforts to solve the structure of the full-length PKG1α.

Experimental procedures

Protein purification

Full-length PKG1α

The full-length protein (human PKG1α$_{2-671}$) was cloned into pBAC1 for insect cell expression as N-terminal 8× histidine fusion protein with a TEV protease site for cleaving the tag. The nucleotide sequence was confirmed by DNA sequencing (Genewiz Inc). The protein was expressed in Sf9 cells supplemented with Sf900 II media (Thermofisher) for 72 h at 27 °C using P2 BIICs at 0.5 multiplicity of infection. For the purification, the insect cell pellet was lysed in 50 mM Hepes, pH 7.5, 300 mM NaCl, 1 mM Tris(2-carboxyethyl) phosphine (TCEP), 1 ml/L protease inhibitor cocktail III (EMD Biosciences), and 5% glycerol. After lysis using a microfluidizer, the lysate was clarified by ultracentrifugation (100,000g for 1 h at 4 °C) and loaded onto a Ni-NTA agarose column pre-equilibrated with lysis buffer. The protein was eluted with 0 to 250 mM imidazole gradient. The fractions containing PKG1α$_{2-671}$ were pooled, concentrated, and further purified using S75 gel filtration column (GE Healthcare). Fractions that showed >95% pure PKG1α$_{2-671}$ based on SDS-PAGE analyses were pooled for storage. The final storage buffer of the protein was 50 mM Hepes, pH 7.5, 200 mM NaCl, 1 mM TCEP, and 10% glycerol. The concentration of the

purified protein was determined using UV spectrophotometry at an extinction coefficient at 280 nm of 75,915 $M^{-1} cm^{-1}$ based on the amino acid sequence of the designed protein construct.

Regulatory domain fragment, PKG1α$_{79-356}$ (CNB sites and switch helix)

The isolated cGMP-binding domain fragment, human PKG1α$_{79-356}$ or bovine PKG1α$_{79-356}$, was cloned into pET47b for bacterial expression as N-terminal 6× histidine fusion protein. The nucleotide sequence was confirmed by DNA sequencing (Genewiz Inc). The protein was expressed in *Escherichia coli* BL21 (DE3) Star cells (Novagen) for 18 h at 16 °C with 1 mM IPTG. For the purification, the bacterial pellet was lysed in 50 mM Hepes pH 7.5, 300 mM NaCl, 5 mM MgCl$_2$, 1 mM TCEP, 1 ml/L protease inhibitor cocktail III (EMD Biosciences) and 5% glycerol. After lysis using a microfluidizer, the lysate was clarified by ultracentrifugation (100,000g for 1 h at 4 °C) and loaded onto a Ni-NTA agarose column pre-equilibrated with lysis buffer. The protein was eluted with 0 to 250 mM imidazole gradient. The fractions containing PKG1α$_{79-356}$ were pooled, concentrated, and further purified using S75 gel filtration column (GE Healthcare). Fractions that showed >95% pure PKG1α$_{79-356}$ based on SDS-PAGE analyses were pooled for storage. The final storage buffer of the protein was 50 mM Hepes pH 7.0, 300 mM NaCl, 5 mM MgCl$_2$, 1 mM TCEP, and 5% glycerol. The concentration of the purified protein was determined using UV spectrophotometry and an extinction coefficient at 280 nm of 31,775 $M^{-1} cm^{-1}$ based on the amino acid sequence of the designed protein construct.

PKG1α ADP-Glo kinase assay

Full-length PKG1α (human PKG1α$_{2-671}$) kinase activity (basal or partially activated by cGMP) in the presence of Glasstide peptide substrate (AnaSpec Inc) and ATP was measured using luminescence-based detection to quantify ADP product formation (ADP-Glo, Promega). Enzyme and substrate working solutions were prepared using the following assay buffer conditions: 50 mM Hepes, 10 mM MgCl$_2$, 150 mM NaCl, 1 mM EDTA, 0.1 mg/ml bovine serum albumin (BSA), 5 mM β-mercaptoethanol (BME), 0.01% Triton X-100, pH 7.3 (BSA, BME, and Triton X-100 were added fresh to stock buffer solution on the day of experiment). Compounds (200 nl in dimethyl sulfoxide [DMSO]) were transferred to 384-well assay plates using Echo acoustic liquid handler (Beckman-Coulter). DMSO (200 nl) and cGMP solution (200 nl, 500 μM) were added to designated control wells on each plate (EC$_{20}$ and EC$_{100}$ control wells, respectively). A solution (8 μl) containing 6.25 nM PKG1α, 187.5 nM Glasstide, and 12.5 nM cGMP was added across all wells. After 30 min incubation at room temperature (RT), 2 μl of ATP solution was added to each well to start the reaction (final assay conditions: 5 nM PKG1α, 150 μM Glasstide, 1 mM ATP, 10 nM cGMP, test compound). After 2 h of incubation at RT, 10 μl of ADP-Glo Max Reagent was added to stop the reaction and

eliminate excess ATP. Following a 40 min incubation, 20 μl of ADP-Glo Max Detection solution was added to the wells. At the end of a 1 h incubation, luminescence signal was read using a PHERAstar Plus (BMG) or Envision (PerkinElmer) plate reader.

Data analysis

Percent PKG1α activation by test compound was calculated relative to baseline (EC$_{20}$ controls) and fully activated signals (EC$_{100}$ controls). EC$_{50}$ values were estimated by fitting % PKG1α activation *versus* compound concentration to a four-parameter activation dose response equation using Abase (IDBS) or PRISM (GraphPad) software.

PKG1α homogeneous time resolved fluorescence assay

Full-length PKG1α (human PKG1α$_{2-671}$) kinase activity was measured using homogeneous time resolved fluorescence method using the homogeneous time resolved fluorescence KinEASE assay kit (CisBio). The assay uses a biotinylated peptide substrate (STK-2), which when phosphorylated is recognized by a monoclonal antiphosphoresidue antibody, labeled with Eu^{3+}cryptate (donor fluorophore). Product detection occurs by an increase in fluorescence signal from streptavidin-XL665 (acceptor fluorophore) that binds to the biotinylated peptide. Enzyme and substrate working solutions were prepared in 50 mM Hepes, 10 mM MgCl$_2$, 150 mM NaCl, 1 mM EDTA, 0.1 mg/ml BSA, 5 mM BME, and 0.01% Triton X-100, pH 7.3. To assess compound activation of partially activated PKG1α, 0.2 μl of compound (50× concentration in DMSO) or 0.2 μl DMSO were dispensed to designated test and EC$_{20}$ control wells, respectively, in a 384-well plate (Corning, catalog no. 3676). A solution (5 μl) containing 10 pM PKG1α, 20 nM cGMP, and 2 μM STK2 peptide was then added to test wells and EC$_{20}$ control wells. The same solution, but with 20 μM cGMP, was added to EC$_{100}$ control wells. After 30 min incubation, 5 μl of 600 μM ATP was added to all the wells to start the reaction (final assay conditions: 5 pM PKG1α, 1 μM STK2 peptide substrate, 300 μM ATP, 10 nM cGMP (in EC$_{20}$ control wells and test field wells), 10 μM cGMP (in EC$_{100}$ control wells), varying concentrations of test compounds and 2% DMSO in assay buffer). The assay plate was then incubated for 30 min at RT. The reactions were quenched and fluorescence signal was developed by adding 10 μl detection solution containing 125 nM streptavidin-XL665 and 2× antibody-cryptate in detection buffer according to manufacturer's protocol. Following 60 min incubation at RT, the emissions at 620 nm and 665 nm were read after excitation at 337 nm using PHERAstar Plus plate reader (BMG).

Data analysis

Percent PKG1α activation by test compound was calculated relative to baseline (EC$_{20}$ controls) and fully activated signals (EC$_{100}$ controls). EC$_{50}$ values were estimated by fitting % PKG1α activation *versus* compound concentration to a four-parameter activation dose response equation using PRISM software.

Microfluidic mobility shift assay

Full-length PKG1α (human PKG1α$_{2-671}$) kinase activity was directly measured using MMSA with a fluorescence-labeled peptide substrate, FL-Peptide 1 (5-FAM-AKRRRLSSLRA-COOH, catalog no. 760345, PerkinElmer) mixed with label-free peptide (AKRRRLSSLRA-COOH, catalog no. 27191, AnaSpec, Inc). Substrate to product conversion was monitored in a Lab-Chip EZ Reader II (PerkinElmer) using a 12-sipper LabChip. Electrophoretic separation of substrate and product used the following separation conditions: downstream voltage –500 V and upstream voltage –2250 V with a screening pressure of –1.9 psi. The amount of product formed was determined according to the following ratio: product peak/(product + substrate peaks). For real time kinetic analysis, the reaction was monitored as it progressed by sequentially sipping samples onto the chip at various time intervals. To estimate the apparent K_M for ATP, initial velocities were measured by assembling reaction solutions in a 384-well plate containing increasing amounts of ATP and 20 nM PKG1α in assay buffer (50 mM Hepes, 10 mM MgCl$_2$, 150 mM NaCl, 0.01% BSA, 1 mM DTT, and 0.01% Triton X-100). The peptide substrate was then added to start the reaction and the assay plate was immediately loaded in the instrument (120 μM final peptide concentration; 1:10 mixture of labeled and unlabeled peptide). The reaction solutions were sampled every 5 minutes for 2 hours at 25 °C. Initial rates were determined from the slopes of the linear regression plots at each ATP concentration and apparent K_M was calculated from nonlinear regression analysis using the Michaelis–Menten equation (PRISM software). To determine K_M for the peptide substrate, solutions containing 20 nM cGMP and various concentrations of peptide (1:10 mixture of labeled peptide and unlabeled peptide) were loaded in a 384-well plate. Saturating ATP was added (1 mM final concentration) to start the reaction. To estimate kinetic parameters, reaction progression curves at varying peptide concentrations were fitted globally using the following GraphPad Prism–based integrated Michaelis–Menten equation described by Zhang and Wong (30) adopted from M. Golicnik (31, 32).

$$Z = S0/Kf * exp((S0 - Vf * X)/Kf)$$
$$S = Kf * (1.4586887 * ln(1.2 * Z/ln(2.4 * Z/ln(1 + 2.4 * Z)))) - 0.4586887 * ln(2 * Z/ln(1 + 2 * Z))$$
$$Y = background + (S0 - S)/S0 * 100$$

As per GraphPad Prism formulation, all subscripts are written without lower offset. Vf and Kf are the maximal steady-state velocities (V) and Michaelis constants (K), respectively. X is the reaction time. Y is the raw turnover kinetics data (% product). $S0$ is the starting substrate concentration constrained as 'equal to the column title' in GraphPad Prism (30).

Microscale thermophoresis

Full-length PKG1α (human PKG1α$_{2-671}$) or regulatory domain fragment (bovine PKG1α$_{79-356}$) was labeled with NT-647-NHS using the Monolith NT Protein Labeling Kit RED-NHS (NanoTemper, L001) following the manufacturer's instructions. Briefly, PKG1α was exchanged and diluted into labeling buffer supplemented with 0.01% Triton X-100 and 0.1 mM TCEP to a final concentration of 16.2 μM for full-length human PKG1α$_{2-671}$ and 43 μM for bovine PKG1α$_{79-356}$ fragment. An equal volume of 43.5 μM NT-647-NHS in the same buffer was added and the resulting solution was incubated at RT for 30 min. Labeled PKG1α was purified by gel filtration into assay buffer (50 mM Hepes, pH 7.3, 150 mM NaCl, 10 mM MgCl$_2$, 1 mM EDTA, 0.01% BSA, 0.01% Triton X-100, and 2 mM TCEP). The final product had a concentration of 3.1 μM or 4.8 μM and was labeled at 1:1.2 or 1:0.94 stoichiometry of PKG1α:NT-647 for (full-length) human PKG1α$_{2-671}$ and bovine PKG1α$_{79-356}$, respectively. For measurements of compound affinity to the target protein, 200 nl of serially diluted compound in DMSO was dispensed to 10 μl of 10 nM protein containing varying concentrations of cGMP in assay buffer. After a 30 min equilibration period, samples were loaded into Monolith NT.115 hydrophilic capillaries (NanoTemper, K004) and read on a Monolith NT.115 instrument using an MST power of 35% for human PKG1α$_{2-671}$ (or 60% for bovine PKG1α$_{79-356}$) and a LED power of 90%. The fluorescence measured after 5 seconds of thermophoresis was fit to a four-parameter dose-response equation in GraphPad Prism in order to determine K_d values.

Fluorescence polarization binding assays

CNB-A and CNB-B competition binding assays using fixed PKG1α and 8-fluo-cGMP concentrations

FP assays were conducted in 50 mM Hepes, pH 7.3, 150 mM NaCl, 10 mM MgCl$_2$, 1 mM EDTA, 0.01% BSA, 0.01% Triton X-100, and 2 mM TCEP in 384-well plates (Corning 4514) using a final volume of 10 μl. The affinity of the FP probe, 8-fluo-cGMP (Biolog Life Sci., Inc), for CNB-A of PKG1α was first determined by mixing 5 μl of a 2× concentration serial dilution of PKG1α with an equal volume of a 2× fixed concentration of the probe. The final concentration of the probe was 0.5 nM ensuring only binding to CNB-A was measured. Binding reactions were incubated at RT for 1 and 3 h, and the polarization state of the probe was measured on a PHERAstar Plus plate reader (BMG). No difference in the observed polarization was noted between the two time points confirming that equilibrium is reached within 1 h. The K_d of 8-fluo-cGMP was determined by fitting the PKG1α concentration response data in GraphPad Prism using a quadratic equation that accounts for ligand depletion as described by Zhang et al. (33). The effect of test compounds on 8-fluo-cGMP binding to CNB-A was determined through equilibrium competition experiments using a fixed concentration of PKG1α (10 nM) and probe (0.5 nM). Briefly, a mixture of PKG1α and probe was added to the assay plate and followed by acoustic dispensing of 200 nl of serially diluted compound in DMSO. The resulting solution was mixed and incubated at RT for 1 h before measuring the polarization of 8-fluo-cGMP using the PheraStar plate reader. Competition experiments using PKG1α loaded with probe at both CNB-A and CNB-B sites were conducted as described above except PKG1α and probe were instead fixed at 100 nM and 200 nM, respectively.

Small molecule allosteric activators of PKG1α

Sequential two-site binding assay

To measure the affinity of 8-fluo-cGMP to the low affinity site (CNB-B) of PKG1α by FP, we devised a novel serial titration scheme. Since practical assessment of probe affinity for the target protein requires that (a) a fixed concentration of probe be used, (b) the concentration of the probe be below the K_d for the target, and (c) a significant fraction of the probe be bound to maximize the dynamic range of the mP signal, typical FP methods cannot measure probe binding to secondary low affinity sites because binding would always be superseded by quantitative binding to the higher affinity site. In order to address this problem, we employed a titration scheme (serial dilution) that simultaneously varied both the PKG1α and probe concentrations while maintaining the ratio of PKG1α and probe fixed at 1:2. This novel scheme allows for the sequential engagement of high and low affinity sites at the relevant concentration range for each binding site as the concentration of both PKG1 and the probe are increased while simultaneously preserving the high fractional binding of the probe required to maximize the dynamic range of the assay.

Experimentally, conditions and procedure were the same as described previously for determination of affinities at CNB-A. Ten microliter of a fixed ratio serial dilution of PKG1α:probe (1:2) was added to the assay plate, followed by acoustic dispensing of 200 nl of compound in DMSO. Each PKG1α:probe concentration condition was read independently and normalized to a well with a matched probe concentration lacking PKG1α. To determine the binding constants for each site from this data, the concentration response curves were fit in Graph-Pad Prism using a set of custom equations; the derivations are outlined as follows for the target protein (P) and ligand (L):
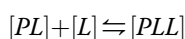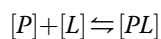
$$[P]+[L] \rightleftharpoons [PL]$$

$$[PL]+[L] \rightleftharpoons [PLL]$$

$$K_d1 = \frac{[P][L]}{[PL]} \tag{1}$$

$$K_d2 = \frac{[PL][L]}{[PLL]} \tag{2}$$

$$[L]_0 = [L] + [PL] + [PLL] \tag{3}$$

$$[P]_0 = [P] + [PL] + [PLL] \tag{4}$$

From Equations 1, 2, and 3, omitting [PL] and [PLL], we obtain

$$[L]_0 = [L] + \frac{[P][L]}{K_d1} + \frac{[P][L]^2}{K_d1K_d2} \tag{5}$$

From Equations 3 and 4

$$[L]_0 - [P]_0 = [L] - [P] \tag{6}$$

From Equations 5 and 6, omitting [P], we obtain

$$[L]^3 + a[L]^2 + b[L] + c = 0 \tag{7}$$

Where

$$a = K_d2 + P_0 - L_0$$

$$b = K_d1K_22 + K_d2(P_0 - L_0)$$

$$c = -L_0K_d1K_d2$$

Solving the physiologically meaningful root of Equation 7, we obtain

$$[L] = -\frac{a}{3} + \frac{2}{3}\sqrt{(a^2 - 3b)}\cos\frac{\theta}{3} \tag{8}$$

Where

$$\theta = arcos\frac{-2a^3 + 9ab - 27c}{2\sqrt{(a^2 - 3b)^3}}$$

The fluorescence polarization as a function of [L], [PL], and [PLL] is equal to

$$Y = \frac{FP_L[L] + \frac{Q_c}{Q_L}FP_{PL}[PL] + 2\frac{Q_c}{Q_L}FP_{PL}[PLL]}{[L] + \frac{Q_c}{Q_L}[PL] + 2\frac{Q_c}{Q_L}[PLL]} \tag{9}$$

Where Y is the total FP value measured, FP_L is the FP value of the free ligand (8-fluo-cGMP), FP_{PL} is the FP value of the protein–ligand complex, and Q_C and Q_L are the molar emissivity of the protein–ligand and unbound ligand, respectively.

The equations, as written in GraphPad Prism, are below.

```
P0 = X
L0 = n*P0
C = -Kd1*Kd2*L0
A = Kd2+P0-L0
B = Kd2*(Kd1+P0-L0)
   Theta = arccos[(-2*A-3 +9*A*B-27*C)/2/
SQRT((A*A-3*B)^3)]
L = -A/3+2/3*SQRT(A*A-3B) * cos(Theta/3)
P = L+P0-L0
C1 = P*L/Kd1
C2 = C1*L/Kd2
   Y = (FP_free*L + FP_bound1*R1*C1
   + FP_bound2*R2*C2)/(L + R1*C1 + R2*C2)
```

¹H STD NMR binding analysis

Ligand binding was detected by STD NMR spectroscopy. The binding buffer contained 25 mM Hepes-d18 (Cambridge Isotope Laboratories), pH 7.3, 150 mM NaCl, 10 mM MgCl$_2$, 2 mM TCEP, 5 μM full-length PKG1α (human PKG1α$_{2-671}$) or isolated regulatory domain (human PKG1α$_{79-356}$) with and without ligands (cGMP, cAMP, or piperidine series activators), and 25 μM TSP in 99.98% D$_2$O. All STD NMR spectra were collected at 298 K on a Bruker 600 MHz Avance spectrometer. Selective saturation of the protein was applied by switching the on- and off-resonance saturation frequency after each scan. A train of Gaussian shape pulses with 50 ms pulse length (corresponding to an excitation width of 100 Hz) separated by a delay of 1 ms was used, with the total length of the selective saturation set to 3 s, and the on- and off-resonance saturation frequencies set to −120 and 20,000 Hz. The total time to acquire one STD NMR dataset, including time to change samples, was 50 min.

Computational modeling methods

Force field

Structures were prepared and refined with the AMBER14:-EHT force field (34, 35).

Site identification

The PKG1α regulatory domain monomer was processed by the Site Finder tool in MOE 2019.0102 (36) and the 5 largest sites were retained for further analysis.

Docking

Molecules were docked using the docking application in MOE 2019.0102 (36) using the triangle matcher placement algorithm with up to 100 poses retained for placement and 50 poses for the final refinement. Molecules were docked to previously identified sites.

Data availability

All data are contained within the manuscript

Abbreviations—The abbreviations used are: AI, autoinhibitory; BME, β-mercaptoethanol; BSA, bovine serum albumin; CNB, cyclic nucleotide binding domain; DMSO, dimethyl sulfoxide; FP, fluorescence polarization; MMSA, microfluidic mobility shift assay; MST, microscale thermophoresis; PKG, cGMP-dependent protein kinase; STD, saturation transfer difference; TCEP, Tris(2-carboxyethyl)phosphine; uHTS, ultrahigh-throughput screening.

References

1. Dang, T. A., Schunkert, H., and Kessler, T. (2020) cGMP signaling in cardiovascular diseases: linking genotype and phenotype. *J. Cardiovasc. Pharmacol.* **75**, 516–525
2. Blanton, R. M. (2020) cGMP signaling and modulation in heart failure. *J. Cardiovasc. Pharmacol.* **75**, 385–398
3. Dunkerly-Eyring, B., and Kass, D. A. (2020) Myocardial phosphodiesterases and their role in cGMP regulation. *J. Cardiovasc. Pharmacol.* **75**, 483–493
4. Preedy, M. E. J., Baliga, R. S., and Hobbs, A. J. (2020) Multiplicity of nitric oxide and natriuretic peptide signaling in heart failure. *J. Cardiovasc. Pharmacol.* **75**, 370–384
5. Sandner, P., Zimmer, D. P., Milne, G. T., Follmann, M., Hobbs, A., and Stasch, J. P. (2021) Correction to: soluble guanylate cyclase stimulators and activators. *Handb. Exp. Pharmacol.* **264**, 425
6. Park, M., Sandner, P., and Krieg, T. (2018) cGMP at the centre of attention: emerging strategies for activating the cardioprotective PKG pathway. *Basic Res. Cardiol.* **113**, 24
7. Kim, G. E., and Kass, D. A. (2017) Cardiac phosphodiesterases and their modulation for treating heart disease. *Handb. Exp. Pharmacol.* **243**, 249–269
8. Ignarro, L. J., and Kadowitz, P. J. (1985) The pharmacological and physiological role of cyclic GMP in vascular smooth muscle relaxation. *Annu. Rev. Pharmacol. Toxicol.* **25**, 171–191
9. Moro, M. A., Russel, R. J., Cellek, S., Lizasoain, I., Su, Y., Darley-Usmar, V. M., *et al.* (1996) cGMP mediates the vascular and platelet actions of nitric oxide: confirmation using an inhibitor of the soluble guanylyl cyclase. *Proc. Natl. Acad. Sci. U. S. A.* **93**, 1480–1485
10. Feil, R., Lohmann, S. M., de Jonge, H., Walter, U., and Hofmann, F. (2003) Cyclic GMP-dependent protein kinases and the cardiovascular system: insights from genetically modified mice. *Circ. Res.* **93**, 907–916
11. Hofmann, F., Bernhard, D., Lukowski, R., and Weinmeister, P. (2009) cGMP regulated protein kinases (cGK). *Handb. Exp. Pharmacol.* https://doi.org/10.1007/978-3-540-68964-5_8
12. Takimoto, E. (2012) Cyclic GMP-dependent signaling in cardiac myocytes. *Circ. J.* **76**, 1819–1825
13. Pfeifer, A., Ruth, P., Dostmann, W., Sausbier, M., Klatt, P., and Hofmann, F. (1999) Structure and function of cGMP-dependent protein kinases. *Rev. Physiol. Biochem. Pharmacol.* **135**, 105–149
14. Moon, T. M., Sheehe, J. L., Nukareddy, P., Nausch, L. W., Wohlfahrt, J., Matthews, D. E., *et al.* (2018) An N-terminally truncated form of cyclic GMP-dependent protein kinase Iα (PKG Iα) is monomeric and autoinhibited and provides a model for activation. *J. Biol. Chem.* **293**, 7916–7929
15. Alverdi, V., Mazon, H., Versluis, C., Hemrika, W., Esposito, G., van den Heuvel, R., *et al.* (2008) cGMP-binding prepares PKG for substrate binding by disclosing the C-terminal domain. *J. Mol. Biol.* **375**, 1380–1393
16. Hofmann, F. (2005) The biology of cyclic GMP-dependent protein kinases. *J. Biol. Chem.* **280**, 1–4
17. Osborne, B. W., Wu, J., McFarland, C. J., Nickl, C. K., Sankaran, B., Casteel, D. E., *et al.* (2011) Crystal structure of cGMP-dependent protein kinase reveals novel site of interchain communication. *Structure* **19**, 1317–1327
18. Moon, T. M., Osborne, B. W., and Dostmann, W. R. (2013) The switch helix: a putative combinatorial relay for interprotomer communication in cGMP-dependent protein kinase. *Biochim. Biophys. Acta* **1834**, 1346–1351

19. Busch, J. L., Bridges, T. M., Richie-Jannetta, R., Hollett, B. P., Francis, S. H., and Corbin, J. D. (2013) Catalytic site amino acids of PKGI-alpha influence allosteric cGMP binding. *Front. Biosci. (Schol Ed.* **5**, 650–660

20. Francis, S. H., Busch, J. L., Corbin, J. D., and Sibley, D. (2010) cGMP-dependent protein kinases and cGMP phosphodiesterases in nitric oxide and cGMP action. *Pharmacol. Rev.* **62**, 525–563

21. Butt, E. (2009) cGMP-dependent protein kinase modulators. *Handb. Exp. Pharmacol.* https://doi.org/10.1007/978-3-540-68964-5_17

22. Moon, T. M., Tykocki, N. R., Sheehe, J. L., Osborne, B. W., Tegge, W., Brayden, J. E., *et al.* (2015) Synthetic peptides as cGMP-independent activators of cGMP-dependent protein kinase Iα. *Chem. Biol.* **22**, 1653–1661

23. Hanisak, J., Soriano, A., Adam, G. C., Basso, A., Bauman, D., Bell, D., *et al.* (2021) Discovery of the first non-cGMP mimetic small molecule activators of cGMP-dependent protein kinase 1 α (PKG1α). *ACS Med. Chem. Lett.* **12**, 1275–1282

24. Francis, S. H., Blount, M. A., Zoraghi, R., and Corbin, J. D. (2005) Molecular properties of mammalian proteins that interact with cGMP: Protein kinases, cation channels, phosphodiesterases, and multi-drug anion transporters. *Front. Biosci.* **10**, 2097–2117

25. Døskeland, S. O., Vintermyr, O. K., Corbin, J. D., and Ogreid, D. (1987) Studies on the interactions between the cyclic nucleotide-binding sites of cGMP-dependent protein kinase. *J. Biol. Chem.* **262**, 3534–3540

26. McCune, R. W., and Gill, G. N. (1979) Positive cooperativity in guanosine 3':5'-monophosphate binding to guanosine 3':5'-monophosphate-dependent protein kinase. *J. Biol. Chem.* **254**, 5083–5091

27. Hofmann, F., and Flockerzi, V. (1983) Characterization of phosphorylated and native cGMP-dependent protein kinase. *Eur. J. Biochem.* **130**, 599–603

28. Kim, J. J., Lorenz, R., Arold, S. T., Reger, A. S., Sankaran, B., Casteel, D. E., *et al.* (2016) Crystal structure of PKG I:cGMP complex reveals a cGMP-mediated dimeric interface that facilitates cGMP-induced activation. *Structure* **24**, 710–720

29. Mak, V. W., Patel, A. M., Yen, R., Hanisak, J., Lim, Y.-H., Bao, J., *et al.* (2022) Optimization and mechanistic investigations of novel allosteric activators of PKG1α. *J. Med. Chem.* https://doi.org/10.1021/acs.jmedchem.1c02109

30. Zhang, R., and Wong, K. (2017) High performance enzyme kinetics of turnover, activation and inhibition for translational drug discovery. *Expert Opin. Drug Discov.* **12**, 17–37

31. Golicnik, M. (2010) Explicit reformulations of time-dependent solution for a Michaelis-Menten enzyme reaction model. *Anal. Biochem.* **406**, 94–96

32. Goličnik, M. (2011) Explicit analytic approximations for time-dependent solutions of the generalized integrated Michaelis-Menten equation. *Anal. Biochem.* **411**, 303–305

33. Zhang, R., Mayhood, T., Lipari, P., Wang, Y., Durkin, J., Syto, R., *et al.* (2004) Fluorescence polarization assay and inhibitor design for MDM2/p53 interaction. *Anal. Biochem.* **331**, 138–146

34. Gerber, P. R., and Müller, K. (1995) MAB, a generally applicable molecular force field for structure modelling in medicinal chemistry. *J. Comput. Aided Mol. Des.* **9**, 251–268

35. Maier, J. A., Martinez, C., Kasavajhala, K., Wickstrom, L., Hauser, K. E., and Simmerling, C. (2015) ff14SB: improving the accuracy of protein side chain and backbone parameters from ff99SB. *J. Chem. Theor. Comput.* **11**, 3696–3713

36. *Molecular Operating Environment (MOE)* 2019.01 Ed.,. (2021) Chemical Computing Group ULC, QC, Canada

ASBMB